Short Communication

Simplified Gas Diffusion Electrode Method for Proton Exchange Membrane Water Electrolysis with a ultralow Pt loading

Xiaofeng Xie, Shusheng Chen, Yuanquan Zhou, Xiaohong Hu[*]

Hubei Key Lab of Electrochemical Power Source, College of Chemistry and Molecular Sciences, Wuhan University. Wuhan Hubei, 430072, China
[*]E-mail: xhhu88@whu.edu.cn

Proton electrolyte membrane water electrolysis is a promising choice of hydrogen energy while limited by the high cost. Low Pt loading and large-scale application are practical for economic consideration. Here we replace the typical hydrophobic agent polytetrafluoroethylene (PTFE) with commercial fluorinated carbon (CFx) to fabricate hydrogen evolution reaction electrodes with a simplified gas diffusion electrode method. The Pt loading can be reduced as low as 0.03 mg cm^{-2} without performance loss, and the electrode fabrication method is easy for mass production. Cyclic voltammetry shows CFx electrode has a high Pt Electrochemical surface area (ECSA) as much as 321 m^2 g^{-1}, and larger than that of PTFE electrode, the Pt utilization increases 12%. Besides, scanning electron microscopy and pore analysis indicate the excellent performance of CFx electrode is related to the more reasonable three-phase boundaries, especially for the improved proton transfer. In addition, the performance differs with the ratio of CFx and content of CFx. We believe the application of CFx in proton exchange membrane water electrolysis has great economic potential due to the ultralow Pt consumption and easy electrode fabrication process.

Keywords: Proton electrolyte membrane water electrolysis; Gas diffusion electrode; Three-phase boundaries; Ultralow Pt loading; Fluorinated acetylene black.

1. INTRODUCTION

Proton electrolyte membrane water electrolysis (PEMWE) has attracted remarkable attention of hydrogen energy due to the higher energy efficiency, hydrogen purity and safety operation for decades, compared with the conventional alkaline water electrolysis and solid state electrolysis. However, it is limited by the high cost of using platinum group metal (PGM, Pt, Ir, Ru) as electrocatalysts and special framework materials [1-3]. Due to the harsh condition of high oxide potential and acidic condition, there is no much choice for anode electrocatalyst. Ir based electrocatalyst is still the best, and frame works are

usually adopted Ti with noble metal (Pt, Au) coated [4]. So low Pt loading and large-scale utilization are favorable of the commercial consideration, as well as in proton exchange membrane fuel cell (PEMFC) [5].

Normally, two ways can be applied to decrease Pt consumption. Some nonnoble catalysts show promising potential of Pt substitution, but the stability of nonnoble catalyst is not satisfied. So Pt is still the best choice for hydrogen evolution reaction (HER) [6-9]. The other one is to increase Pt utilization. Except developing higher catalytic activity Pt nanoparticles, an effective three-phase boundaries electrodes is always preferred [10-12]. Fabricating an effective three-phase boundary electrode is always closely linked to the membrane electrode assembly (MEA) method and the electrode fabrication method [13]. As taking PTFE as binder, the first generation of three-phase boundaries electrodes fabricated by gas diffusion electrode (GDE) method have a high Pt loading of 4-10 mg cm^{-2} and a low Pt utilization of 20% [14]. The catalyst coated membrane (CCM) method increases Pt utilization to 45% by improving the proton transfer between membrane and catalyst layer (CL) [15]. Electrode made by this method usually has a thin CL, also called as thin film electrode. Since CCM method is developed, PTFE is rarely used in the CL. Despites CCM method is widely used, it still suffers the default of a complex manufacturing process and the difficulty of achieving uniformity in large-scale production. [16-20].

Coating PTFE or other hydrophobic polymers changes the wetting properties of carbon materials, so does fluorination [21-23]. Tristan Asset et al. show Pt supported by fluorinated carbon is more anti-corrosion, compared with bare carbon [24, 25]. Low-molecular-weight PTFE powder in CL is proofed improving the oxygen transport resistance of PEMFC [26]. While no study has investigated the application of hydrophobic fluorinated carbon on PEMWE, and no effort is made to eliminate the defect of PTFE in traditional GDE. Given the hydrophobicity of fluorinated carbon and easier GDE fabrication method, we propose that replacing PTFE with CFx may make up the loss of low Pt utilization in the traditional GDE. This time, we used commercial fluorinated acetylene black (CFx, x = 0.9, x indicates the fluorination level) to replace PTFE.

2. MATERIAL AND METHODS

2.1 CFx characterization

The analysis of the purchased CFx was performed by X-ray diffraction (XRD, XRD-600, SHIMADZU, Japan), scanning electron microscopy (SEM, SUPRA 55, ZEISS, Germany) and cyclic voltammetry (CV). Modified glassy carbon electrodes (GCEs) made by casting a mixture of CFx (Hubei Zhuoxi Fluorochemical Co. Ltd. China), Nafion solution (5% wt. DuPont de Nemours and Company, USA) with or without Pt/C (Pt 20% wt.) on a 3 mm diameter GCE was utilized as work electrode (WE). A Pt-Ti slice and a mercurous sulfate electrode (MSE *VS.SHE* 0.64 V) served as counter electrode (CE) and reference electrode (RE) respectively. A 2 mol L^{-1} H$_2$SO$_4$ solution was utilized as electrolyte. CV was carried out by CHI660e (CH Instruments Ins. USA), scanned from -0.6 to -0.8 V *VS.MSE* at a scan rate of 0.05 V s^{-1}.

2.2 Electrode fabrication

Catalyst inks were prepared by mixing Pt/C (Pt 20% wt.), Nafion ionomer (5% wt.), PTFE suspension (60% wt.) or CFx, isopropanol and deionized water. Following ultrasonication, PTFE catalyst ink was sprayed on a self-humidified and wet-proof carbon paper by an air-powered spray gun [10]. The CFx electrodes were made by spreading 300 μL CFx-contained catalyst ink on the same carbon paper [27]. Then the electrodes were dried at 130 °C in air. The electrodes contained 20%, 40% and 60% CFx were labelled as CFx-20, CFx-40 and CFx-60 respectively. Nafion ratio was fixed on 20%. An acetylene black electrode also was made with the same method of CFx electrode.
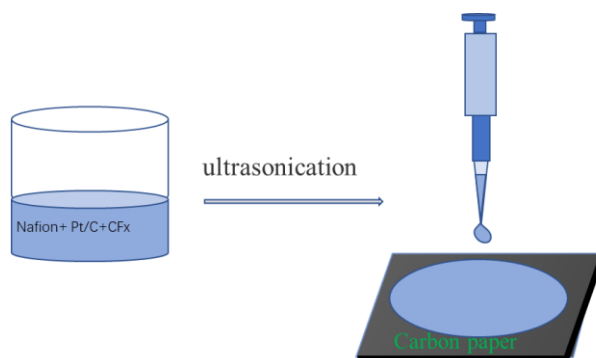

Figure 1. Schematic of CFx electrode fabrication.

2.3 Electrode characterization

Morphology of electrode surface was characterize by SEM (SUPRA 55, ZEISS, Germany). Electrode pore parameters was got by a mercury porosimeter (Autopore IV 9500, Micromeritics, USA), including total pore area, average pore size, porosity, and tortuosity [28].

The Pt electrochemical surface area (ECSA) of electrodes was calculated by CV method. Electrolyzer was composited with two fabricated Pt/C electrodes at the sides of Nafion membrane. One side was CFx electrode and other side was PTFE electrode. When CV tests were conducted, one chamber was inlet with moist hydrogen, and the corresponding electrode was served as reference electrode and counter electrode. The other chamber was inlet with wet high-pure argon and the electrode utilized as work electrode. Then the scanned from 0.05 to 1.2 V with a rate of 20 mV s^{-1}. The fifth cycle was chosen to calculate Pt ECSA from 0.05 to ~ 0.4 V (double layer region) [29, 30].

2.4 Performance of electrodes

Electrolyzer was assembled with a fabricated HER electrode, an 8 cm^2 anode electrode and a well-treated Nafion®-117 membrane as Ref. [31]. Anode electrode was composed of an anti-corrosion porous titanium gas diffusion layer (GDL) and a CL contained 15% Nafion, 5% PTFE and 80% IrO$_2$,

the IrO$_2$ loading was 5 mg cm^{-2}. Lifetime tests and polarization curves were conducted by a direct current power supply. A heater was utilized to control the temperature of feed water.

3. RESULTS AND DISCUSSION

The characterization of commercial CFx is showed in Fig. 2. XRD analysis (Fig. 2a) showed the typical broad peaks centered at 13°, 26° and 41° were corresponded to the fluorinated phases [32]. SEM image (Fig. 2b) indicated the particle size of CFx was 50-60 nm on average. CV curves (Fig. 2c) implied CFx had no hydrogen evolution activity. Obviously, CFx itself makes no contribution to HER. In addition, CFx can be dispersed uniformly in Nafion solution, as Fig. 2d shown. Electrochemical reaction is proceeded at the three-phase boundaries. Except the choice of electrocatalyst, the electrode structure is proofed impacts the performance of electrolyzer greatly. An orderly distribution of electron conductor (maintained by electrocatalyst), ionic passage (Nafion is preferred) and gas channel (supported by hydropholic agent) is important to the performance too [33, 34]. Compared with network structure PTFE, power sized CFx is more competitive to get a uniform distribution with Pt/C and Nafion ionomer. Thus means more reasonable three-phase boundaries can be formed in the CL of CFx electrode.
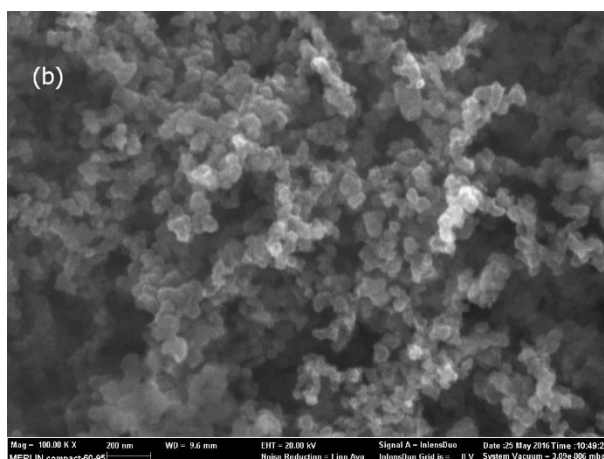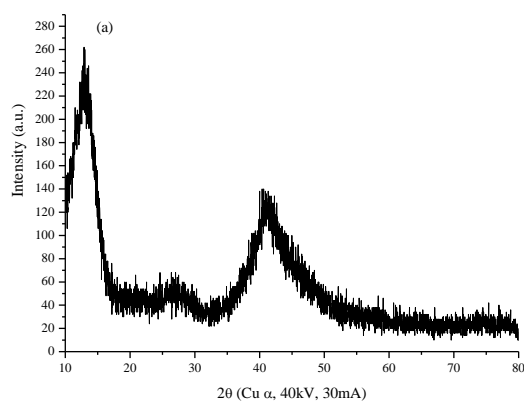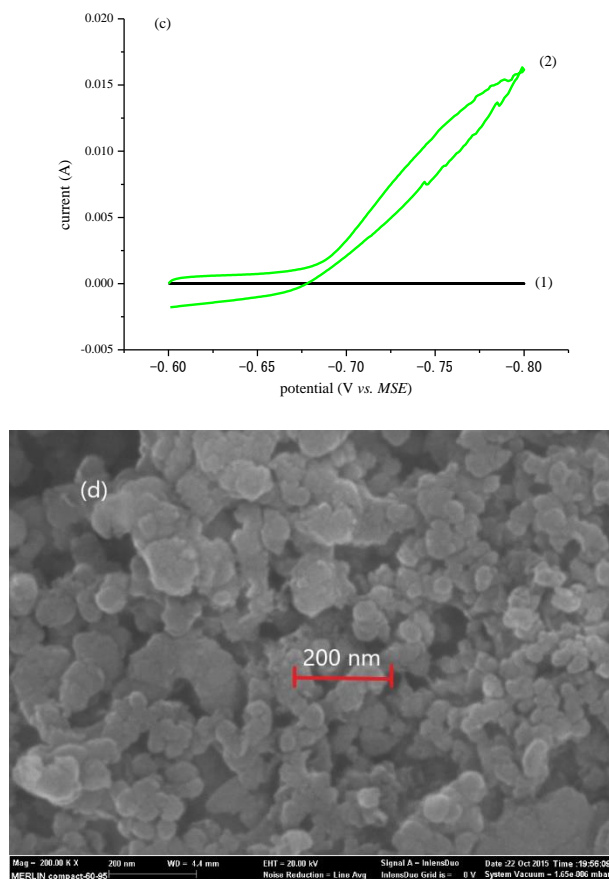
Figure 2. Characterization of CFx. (a) XRD patterns of CFx. (b) SEM image of CFx. (c) CV curves. GCEs were used as WE, a Pt slice was taken as CE and a MSE was utilized as RE. A 2 mol L^{-1} H$_2$SO$_4$ was served as electrolyte, scanned from -0.6 to -0.8 V *VS.*$_{MSE}$ at a scan rate of 0.05 V s^{-1}. (1) Modified GCE contains 80% CFx, 20% Nafion. (2) Modified GCE contains CFx 20%, Pt/C 60%, Nafion 20%. (d) SEM image of CFx (20%) mixed with Nafion (80%).

Fig. 3 exhibited the morphology of electrode surface. Obviously, PTFE-bound electrode (Fig. 3a) had an irregular particle distribution, and particles were distributed unevenly, some Pt/C even were covered by PTFE. Air-driven spraying suffers an agglomeration of nanoparticles. An unsmooth surface can be formed at the substrate, which is unbeneficial to build a connective proton transportation between membrane and CL [34]. Besides, some Pt particles are covered, which may decrease reaction sites. Spraying method is easy to get a thin CL, but spay catalyst ink on carbon paper goes against to create an inefficient interface between membrane and CL, thus catalyst ink is normally sprayed on the membrane. Also, the network and chain structure of PTFE makes it uneasy to disperse uniformly, a repeated rolling or other mechanical methods can, but it is difficult to get a thin CL. In a word, electrode with high performance and low Pt loading is always accompanied with a thin CL and efficiency three-phase boundaries.

A thin CL can be obtained easily by a proper coating. Dropping several microliters of the CFx catalyst ink on a tin foil gets a few-micron-thin coating, as well as with a smooth surface, seen in Fig. S1, indicates the CFx electrodes might have a thin catalyst layer with a uniform surface too. Different

with PTFE, the nano particle sized CFx can be more uniformly distributed after ultrasonication. For CFx electrode, the force of dispersing catalyst ink is gentle, which is benefit of creating a smooth surface. In addition, the simplified gas diffusion electrode fabrication had an economic advantage of large-scale manufacture. Considering the mention reasons, CFx is a competitive alternative of PTFE in PEMWE for hydrogen evolution reaction electrode fabrication.
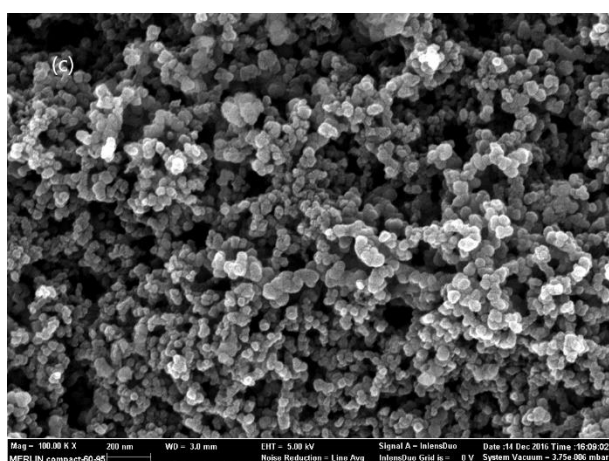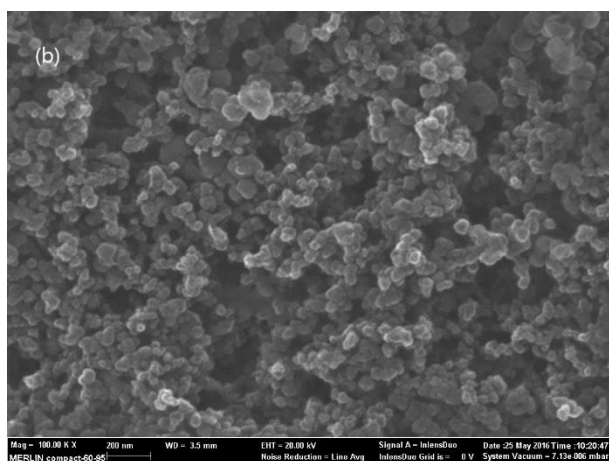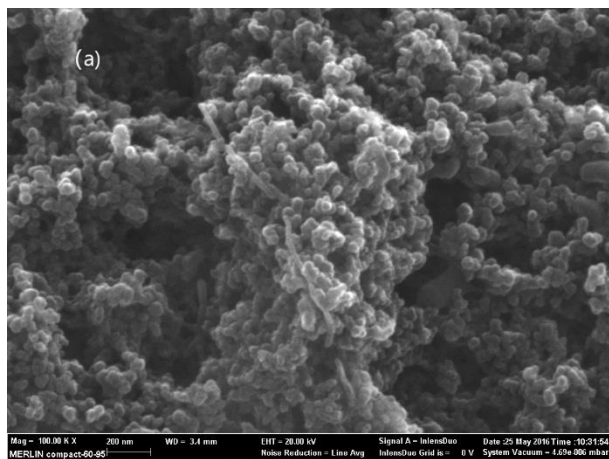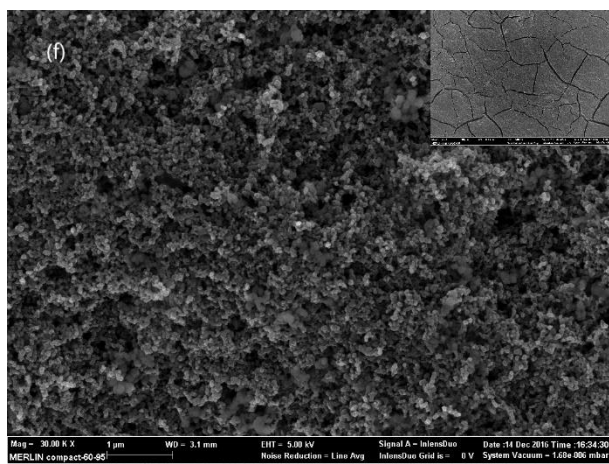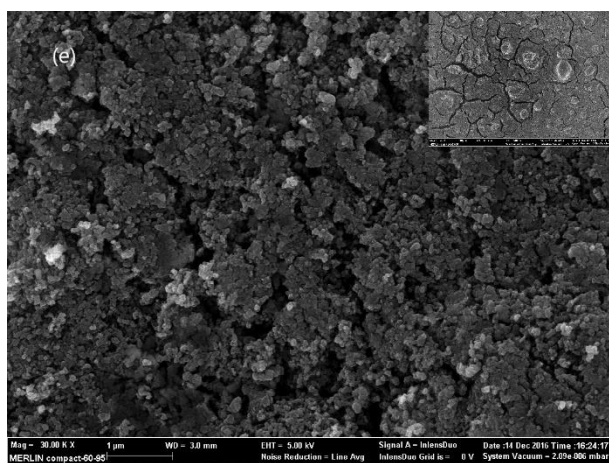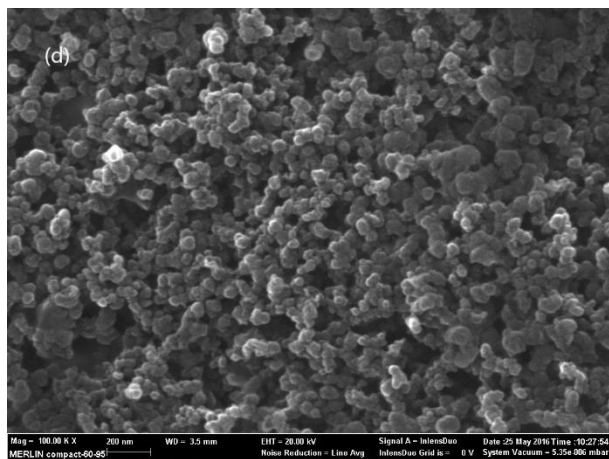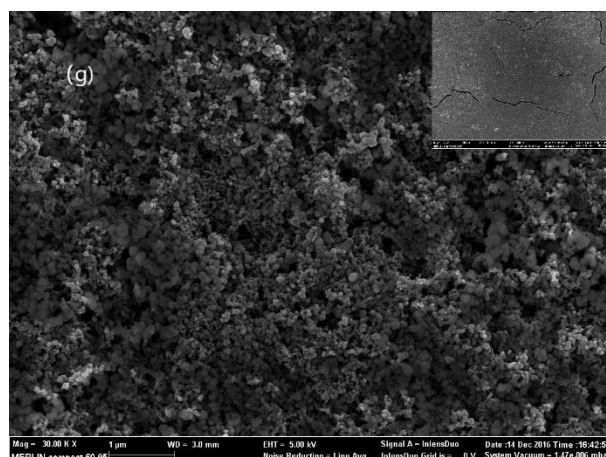
Figure 3. SEM images of fabricated electrodes. (a) PTFE-20 with high weight CL. (b) CFx-20 with high weight CL. (c) CFx-40 with high weight CL. (d) CFx-60 with high weight CL. (e) CFx-20 with low weight CL. (f) CFx-40 with low weight CL. (g) CFx-60 with low weight CL.

Despites the potential of fabricating a good performance electrode, SEM results (Fig. 3b to Fig. 3g) and pore analysis (Table 1) indicated not all the CFx electrodes had a beneficial three-phase boundaries. The ratio and content of CFx significantly impacted the morphology and pore structure of CL.

There was no evident difference between the high weight CL electrodes. While cracks were clearly observed on CFx-20 electrode with low weight CL. Cracking is more serious in an aggregated CL [35]. Obviously, aggregation misses the goal of uniform three-phase boundaries. The reason why CFx-20 electrode with low weight CL had the most cracks in CL was unclear. We speculated the composition of catalyst ink affects the particle stacking. The catalyst inks are mixed with a fixed solvent (water and isopropanol) and various solutes (CFx, Pt/C and Nafion). It seems more Pt/C makes the catalyst ink denser, which is unhelpful for dispersion. We might prepare a thinner catalyst ink for CFx-20 electrode, which means more solution should spread on carbon paper with the same loading. However, 250 - 350 μL catalyst ink is suitable to overspread a 9 cm^2 carbon paper.

Pore analysis (Table 1) provided a detail pore characterization of the electrodes. These electrodes shared the same porosity, but inner pore structure varies with each other. Carbon paper acting as GDL, is rich of macropores, has the largest average pore diameter. CL, a micropore layer, has a much less thickness than the GDL, which means most of pore volume is local in GDL, so the porosity rarely changes. SEM images has verified PTFE-bound electrode has an irregular particle distribution, so its tortuosity mostly increases. Micropore in CL rises the total pore area of the electrode, also reduces the average pore diameter. Generally, an orderly particle stacking has more pore area [20]. Higher total pore area indicates more exposed area and active sites, which improves Pt utilization. While the reward reduces at high weight CL, the situation is especially serious for CFx-60, nearly has no contribution to create more active sites.

Table 1. Pore analysis of electrodes, the area of electrode was 8 cm^2.

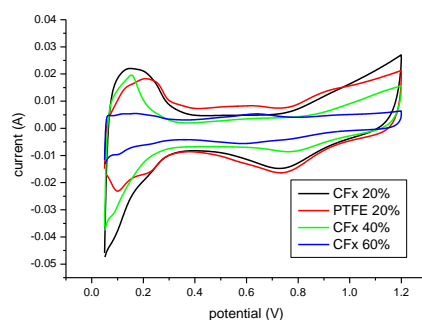|	CL weight (mg)	Porosity (%)	Total pore area (m^2 g^{-1})	Average pore diameter (nm)	Tortuosity
GDL[a]	0	65	16.1	226	3.7
CFx-20	6.5	58	17.1	211	4.0
CFx-20	10.2	60	19	178	3.5
PTFE-20	10.2	63	16.2	200	5.7
CFx-20	14.9	59	21.5	154	3.9
CFx-40	6.5	58	16.5	200	4.1
CFx-40	10.2	64	22	155	3.9
CFx-40	14.9	64	20.8	175	4.1
CFx-60	6.5	61	17.6	178	3.4
CFx-60	10.2	60	22	137	4.6
CFx-60	14.9	63	13.4	246	4.5

GDL[a] represents carbon paper.

Figure 4. CV curves. One chamber was inlet with moist hydrogen, and the corresponding electrode was served as reference electrode and counter electrode. The other chamber was inlet with wet high-pure argon and the electrode utilized as work electrode. Then the scanned from 0.05 to 1.2 V with a rate of 20 mV s^{-1}.

Except the characterization of electrode structure indicated CFx electrode had a potential of lowing Pt loading, CV tests also confirmed. Fig. 4 showed CV results and Table 2 listed the Pt ECSA of the electrodes. Pt ECSA can be calculated from Eq. (1) [30, 36]

$$ECSA(m^2 \cdot g^{-1}) = \frac{S_H/V}{0.21(C \cdot m^{-2}) \cdot M_{Pt}} \qquad (1)$$

S_H is the area of hydrogen underpotential adsorption/deposition peaks, double layer region is excluded. V presents scan rate, 20 mV s^{-1}. And 0.21 (C m^{-2}) is the charge of Pt surface fully covered with monolayer H. M_{Pt} is the mass of Pt. Compared with PTFE-bound electrode, Pt utilization of CFx electrode increased

at least 12%, and the ECSA was 5-7 times bigger than the commercial Pt/C. Most commercial Pt/C (Pt 20%) has an ECSA of 50-70 m^2 g^{-1} [37, 38]. And the CFx-20% has the highest Pt ECSA due to the highest Pt loading. However, the later polarization showed CFx-60% had the best performance, which went against CV results. Pt ECSA cannot reflect the real situation of water electrolysis. And this method is more adopted to fuel cell system. In the fuel cell system, gas/water transportation is more concerned, while in electrolysis system, mass transportation is not focused.

Table 2. ESCA calculated from CV results.

	Pt loading (mg cm^{-2})	Pt ECSA (m^2 g^{-1})
CFx-60%	0.03	321
CFx-40%	0.06	349
CFx-20%	0.09	369
PTFE-20%	0.09	286

Fig. 5 showed the polarization curves of the electrolyzers. CFx electrode had a better performance than that of PTFE-bound electrode at low temperature and high current density with the same Pt loading and weight content of hydrophobic agent, seen as Fig. 5a. Cell voltage (*U*) can be expressed as Eq. (1).

$$E^\theta = E^\theta_{\varphi a} + \eta_a - E^\theta_{\varphi c} + \eta_c + iR \qquad (2)$$

E_θ also represents the energy consumption [39]. In this paper, the electrocatalysts are the same, so the difference of cell voltage is mainly related to *iR*. *iR* reflects the resistance of electron, proton and mass transportation. Normally, Running at 2 A cm^{-2} suffers no serious mass polarization. In the CL, Nafion, CFx or PTFE are electron nonconductors, Pt/C is responsible for electron transportation. A reasonable particle stacking means a lower electron resistance. Proton conduction is supported by Nafion ionomer. A more connective proton channel would be built between membrane and CL on the condition of a smooth CL, especially running at low temperature and high current density the proton transfer would be more impeded. Three-phase boundaries of CL are the main place where electrochemical reaction goes on. It is the effective three-phase boundaries of CFx electrode contributes to the excellent performance.

Luckily, the Pt loading can be reduced lower, even lower than 0.03 mg/cm^2, much lower than the requirement of US department of energy for PEMFC, 0.125 mg cm^{-2} [40]. For those CFx electrodes, the performance is similar at 80 °C and 1 A cm^{-2}. However, CFx-60 with low weight CL had a stable cell voltage increase at low temperature and high current density, seen from Fig. 5b and Fig. 5c. Despites CFx-20 has a good performance at high temperature, but it is contrary to the economic consideration. SEM results and pore analysis have indicated CFx-60 with low weight CL has an advantageous electrode structure, so there is no doubt it has a more outstanding performance.
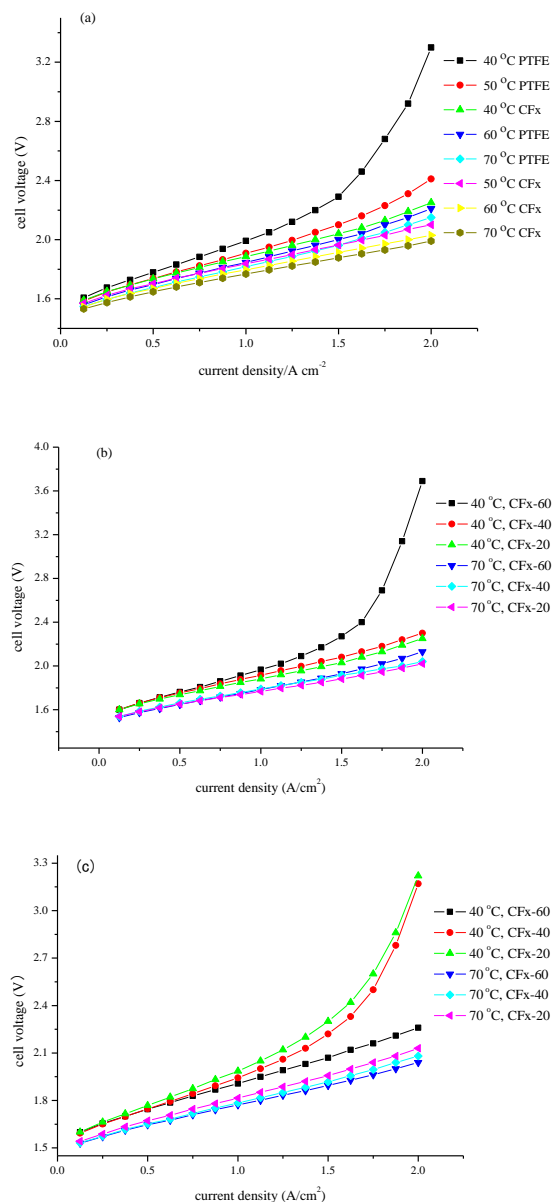
Figure 5. Polarization curves. (a) Polarization curves of PTFE-20 and CFx-20 (Pt loading of 0.12 mg/cm^2) at 40 °C and 70 °C. (b) Polarization curves of CFx electrodes with CL weights of 12.9 mg at 40 °C and 70 °C. (c) Polarization curves of CFx electrode with CL weights of 5.7 mg at 40 °C and 70 °C.

Also, we prepared an acetylene black electrode (60% acetylene black, 20% Pt/C and 20% Nafion, Pt loading: 0.03 mg cm^{-2}) which had the same fabrication method with CFx electrode. Fig. 6 showed the characterization of acetylene black electrode. SEM images Fig. 6a exhibited the unsmooth surface of the acetylene black electrode. Of course, the performance was terrible, even was worse than that of PTFE electrode. When running at low temperature, the situation was more serious. The role of CFx was non-negligible. The distribution of CL particle is more reasonable with the presence of CFx.
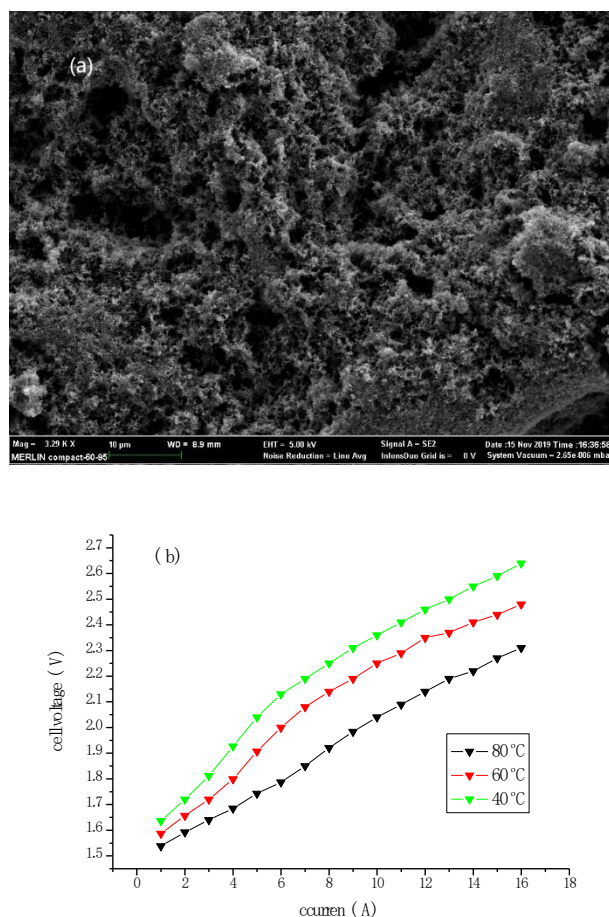
Figure 6. Characterization of acetylene black electrode (60% acetylene black, 20% Pt/C and 20% Nafion, Pt loading: 0.03 mg cm^{-2}). (a) SEM images. (b) Polarization curves.

4. CONCLUSION

Commercial CFx as hydrophobic agent to replace traditional PTFE for HER electrode fabrication in PEMWE was studied. PTFE-bound electrode and CFx electrode were fabricated by spraying method and spreading method respectively. SEM and pore analysis showed CFx electrode had a more effective three-phase boundaries, compared with PTFE-bound electrode. Also CFx-60 electrode with a low weight CL had the best performance with a low Pt loading of 0.03 mg cm^{-2}. Besides, the performance of CFx electrodes differed with the content and ratio of CFx. We believe the application of CFx in PEMWE for HER has economic benefit of the low Pt loading and simplified electrode fabrication.

Of course, this work needs further investigation. For example, 20% Nafion may not the best ratio. And there is various kinds of fluorinated carbon, does the carbon source and fluorination degree differ the performance? Fluorinated carbon as Pt support and fluorinated graphite as GDL improve the performance of PEMFC, can our CFx electrode have a remarkable performance on PEMFC too?

References

1. M. Momirlan and T. V. Veziroglu, *Renew. Sust. Energy Rev.,* 6 (2002) 141.
2. O. Schmidt, A. Gambhir, I. Staffell, A. Hawkes, J. Nelsona and S. Few, *Int. J. Hydrogen Energy,*

42 (2017) 30470.

3. A. Buttler and H. Spliethoff, *Renew. Sust. Energy Rev.,* 82 (2018) 2440.
4. Q. Feng, X. Yuan, G. Liu, B. Wei, Z. Zhang, H. Li and H. Wang, *J. Power Sources,* 366 (2017) 33.
5. U. Babic, M Suermann, F. N. Büchi, L. Gubler and T. J. Schmidt, *J. Electrochem. Soc.,* 164 (2017) F387.
6. S. M. S. Kumar, K. Selvakumar, R. Thangamuthu, A. K. Selvi, S. Ravichandran, G. Sozhan, K. Rajasekar, N. Navascues and Silvia Irusta, *Int. J. Hydrogen Energy,* 41 (2016) 13331.
7. M. A. Khan, H. Zha, W. Zou, Z. Chen, W. Cao, J. Fang, J. Xu, L. Zhang and J. Zhang, *Electrochem. Energy Rev.,* 1 (2018) 483.
8. J. Deng, P. Ren, D. Deng, L. Yu, F. Yang and X. Bao. *Energy Environ. Sci.,* 7 (2014) 1919.
9. A. Ganassin, V, Colic, J. Tymoczko, A. S. Bandarenka and W. Schuhmann, *Phys. Chem. Chem. Phys.,* 17 (2015) 8349.
10. M. Carmo, D. L. Fritz, J. Mergel and D. Stolten, *Int. J. Hydrogen Energy,* 38 (2013) 4901.
11. D. Strmcnik, P. P. Lopes, B. Genorio, V. R. Stamenkovic and N. M. Markovic, *Nano Energy,* 29 (2016) 29.
12. S. Litster and G. McLean, *J. Power Sources,* 130 (2004) 61.
13. S. Siracusano, N. V. Dijk, R. Backhouse, L. Merlo, V. Baglio and A. S. Aricò, *Renew. Energy,* 123 (2018) 52.
14. X. Cheng, B. Yi, M. Han, J. Zhang and Y. Qiao, *J. Power Sources,* 79 (1999) 75.
15. M. S. Saha, A. F. Gullá, R. J. Allen and S. Mukerjee, *Electrochim. Acta,* 51 (2006) 4680.
16. T. Huang, H. Shen, T. Jao, F. Weng and A. Su, *Int. J. Hydrogen Energy,* 37 (2012) 13872.
17. S. Thanasilp and M. Hunsoma, *Fuel,* 89 (2010) 3847.
18. E. Zamburlinia, K. D. Jensena, I. E. L. Stephens, I. Chorkendorff and M. Escudero-Escribano, *Electrochimi. Acta,* 247 (2017) 708.
19. A. Lindermeir, G. Rosenthal, U. Kunz and U. Hoffmann, *J. Power Sources,* 129 (2004) 180.
20. D. S. Hwang, C. H. Park, S. C. Yi and Y. M. Lee, *Int. J. Hydrogen Energy,* 36 (2011) 9876.
21. T. V. Nguyen, A. Ahosseini, X. Wang, V. Yarlagadda, A. Kwong, A. Z. Weber, P. Deevanhxay, S. Tsushima and S. Hirai, *J. Electrochem. Society,* 162 (2015) F1451.
22. A. Tressaud, E. Durand, C. Labrugère, A. P. Kharitonov and L. N. Kharitonova, J. Fluorine Chem., 128 (2007) 378.
23. H. Muramatsu, Y. A. Kim, T. Hayashi, M. Endo, A. Yonemoto, H. Arikai, F. Okino and H. Touhara, *Chem. Commun.,* 15 (2005) 2002.
24. J. L. Bott-Netoa, T. Asseta, F. Maillard, L. Dubau, Y. Ahmad, K. Guérin, S. Berthon-Fabry , A. Mosdale, R. Mosdale, E. A. Ticianelli and M. Chatenet, *J. Power Sources,* 404 (2018) 28.
25. T. Asset, B. R. Chattot, F. Maillard, L. Dubau, Y. Ahmad, N. Batisse, M. Dubois, K. Guérin, F. Labbé, R. Metkemeijer, S. Berthon-Fabry and M. Chatenet, *J. Electrochem. Society,* 165 (2018) F3346.
26. S. Wang, X. Li, Z. Wan, Y. Chen, J. Tana and M. Pan, *J. Power Sources,* 379 (2018) 338.
27. S. Gamburzev and A. J. Appleby, *J. Power Sources,* 107 (2002) 5.
28. L. Cindrella, A. M. Kannan, J. F. Lin, K. Saminathan, Y. Ho, C. W. Lin and J. Wertz, *J. Power Sources,* 194 (2009) 146.
29. J. Wu, X. Z. Yuan, H. Wang, M. Blanco, J. J. Martin and J. Zhang, *Int. J. Hydrogen Energy,* 33 (2008) 1735
30. K. Shinozaki, Y.Morimoto, B. S. Pivovar and S. S. Kocha, *J. Power Sources,* 325 (2016) 745.
31. S. Chen, F. Jiang, X. Xie, Y. Zhou and X. Hu, *Electrochi. Acta,* 192 (2016) 357.
32. W. J. Yang, Y. Dai, S. D. Cai, Y. Zheng, W. Wen, K. Wang, Y. Feng and J. Xie, *J. Power Sources,* 255 (2014) 37.
33. J. Moreira, A. L. Ocampo, P. J. Sebastia, M. A. Smit, M. D. Salazar, P. del Angel, J. A. Montoya, R. Pérez and L. Martínez, *Int. J. Hydrogen Energy,* 28 (2003) 625.

34. H. Liang, H. Su, Bruno, G. Pollet and S. Pasupathi, *J. Power Sources,* 288 (2015) 121.
35. N. Kumano, K. Kudo, A. Suda, Y. Akimoto, M. Ishii and H. Nakamura, *J. Power Sources,* 419 (2019) 219.
36. S. Torija, L. Prieto-Sanchez and S. J. Ashton, *J. Power Sources,* 327 (2016) 543.
37. H. Lee, Y. Sung, I. Choi, T. Lim and O. J. Kwon, *J. Power Sources,* 362 (2017) 228.
38. L. Chinchilla, D. Rossouw, T. Trefz, D. Susac, N. Kremliakova and G. A. Botton, *J. Power Sources,* 356 (2017) 140.
39. L. Ma, S. Sui and Y. Zhai, *Int. J. Hydrogen Energy,* 34 (2009) 678.
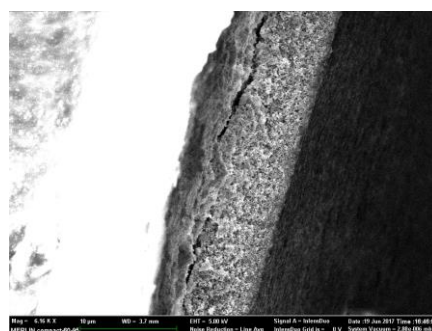40. Y. Garsany, R. W. Atkinson III, B. D. Gould and K. E. Swider-Lyons, *J. Power Sources,* 408 (2018) 38.

Figure S1 SEM images of tin foil coated with several μL CFx catalyst ink.